analytical chemistry

pubs.acs.org/ac Article

Ultrasensitive and Selective Determination of Carcinoembryonic Antigen Using Multifunctional Ultrathin Amino-Functionalized Ti_3C_2-MXene Nanosheets

Qiong Wu, Ningbo Li, Ying Wang, Yanchao Xu, Jiandong Wu, Guangri Jia, Fujian Ji, Xuedong Fang,* Fangfang Chen,* and Xiaoqiang Cui*

Cite This: https://dx.doi.org/10.1021/acs.analchem.9b05372 Read Online

ACCESS | Metrics & More | Article Recommendations | Supporting Information

ABSTRACT: Herein, we report on a two-dimensional amino-functionalized Ti_3C_2-MXene (N−Ti_3C_2-MXene)-based surface plasmon resonance (SPR) biosensor for detecting carcinoembryonic antigen (CEA) utilizing a sandwich format signal amplification strategy. Our biosensor employs an N-Ti_3C_2-MXene nanosheet-modified sensing platform and a signal enhancer comprising N-Ti_3C_2-MXene-hollow gold nanoparticles (HGNPs)-staphylococcal protein A (SPA) complexes. Ultrathin Ti_3C_2-MXene nanosheets were synthesized and functionalized with aminosilane to provide a hydrophilic-biocompatible nanoplatform for covalent immobilization of the monoclonal anti-CEA capture antibody (Ab_1). The N-Ti_3C_2-MXene/HGNPs nanohybrids were synthesized and further decorated with SPA to immobilize the polyclonal anti-CEA detection antibody (Ab_2) and serve as signal enhancers. The capture of CEA followed by the formation of the Ab_2-conjugated SPA/HGNPs/N-Ti_3C_2-MXene sandwiched nanocomplex on the SPR chip results in the generation of a response signal. The fabricated N-Ti_3C_2-MXene-based SPR biosensor exhibited a linear detection range of 0.001−1000 PM with a detection limit of 0.15 fM. The proposed biosensor showed high sensitivity and specificity for CEA in serum samples, which gives it application potential in the early diagnosis and monitoring of cancer. We believe that this work also opens new avenues for development of MXene-based highly sensitive biosensors for determining various biomolecules.

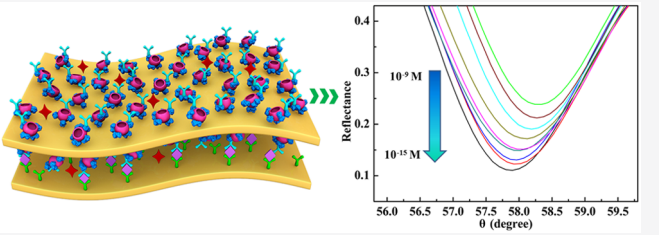

Carcinoembryonic antigen (CEA), a kind of glycoprotein, is recognized as the most common biomarker for cancers. The CEA level in serum is of great reference significance to the clinical cancer diagnosis.[1] Developing a sensitive and selective method for determining CEA is very meaningful for early treatment of cancers with relatively good prognosis and improvement of survival duration. Currently, in virtue of development of analytical techniques, many methods have been reported to detect CEA in real samples. These techniques include enzyme-linked immunoassay (ELISA),[2] photoelectrochemical immunoassay,[3] fluoroimmunoassay,[4] electrochemiluminescence,[5] and electrochemical immunoassay.[6] However, new methods of low cost, easy operation, and high sensitivity are still required for applications in clinical diagnosis.

Surface plasmon resonance (SPR) sensing technology provides a sensitive real-time response to the binding of chemical and biomolecules of interest to the sensing chip surface without labeling. The advantages of high sensitivity and specific detection of low-concentration target analytes in complex matrices make it a powerful tool in various application fields including biological analysis,[7] food safety and supervision,[8] disease diagnosis and control,[9] and environmental monitoring.[10] However, its inadequate sensitivity for detecting analytes with low molecular weight or at extremely dilute concentrations has become a bottleneck for the further development of SPR biosensing technology.[11] To overcome this challenge, sensor surface modification through the introduction of nanoparticles has been proposed for SPR signal enhancement.[12,13] Various nanomaterials have been utilized in SPR biosensing owing to their intrinsic advantages over conventional sensing materials, including large surface areas, small sizes, high specificity, good biocompatibility, and photostability.[14] Nanomaterial-enhanced SPR systems have exhibited better performances than conventional SPR systems and broad application prospects.[15−17] With the development of nanomaterials, many new two-dimensional (2D) materials such as graphene and its derivatives,[13] MoS_2,[18] black phosphorus (BP),[19] and antimonene[20] have been discovered, which have greatly accelerated the development and application of biosensing technology. Recently, a new family of 2D layered materials, transition-metal carbides and carbonitrides materials named MXenes, have received

Received: November 27, 2019
Accepted: January 27, 2020

considerable attention.[21−23] MXenes are generally prepared by etching sp element layers from the corresponding 3D MAX phases, and they exhibit a semblable morphology of exfoliated graphite.[24] MAX phases are layered ternary metal carbides, nitrides, or carbonitrides with a general formula $M_{n+1}AX_n$ (n = 1, 2, 3), where M corresponds to early d-block transition metals such as Ti, Sc, V, Cr, Ta, and Nb. Here, A corresponds to main group sp elements designated as groups 13 and 14, and X corresponds to a C or N atom.[25] The MXenes generally exhibit metallic conductivity and good hydrophilicity, making them good for catalysis,[26] biosensors,[27] energy storage, supercapacitors,[28] and lithium ion batteries.[29] For MXenes, the abundant oxygen or hydroxyl functional groups and complete metal atomic layers endow them with the ability of interacting with plentiful biomolecules and for utilization as nanobiointerface units for biosensing.[24] Few-layer Ti_3C_2-MXene, a new biosensing material, has exhibited superior capacity for loading biomolecules and has become a recent hot spot. To date, Ti_3C_2-MXene-based electrochemical, electrogenerated chemiluminescence (ECL), and fluorescent biosensors have been reported.[30−32] It should be noted that MXenes similar to most nanomaterials also suffer from aggregation and precipitation in complex matrixes especially biological mediums. Surface engineering is a critical way to improve the stability of these nanosystems by decorating other functional materials.[33]

In this paper, amino group-functionalized single/few-layered Ti_3C_2-MXene nanosheets were assembled on the surface of a thin gold film as the sensing material for the covalent immobilization of monoclonal anti-CEA antibodies (Ab_1). Furthermore, N-Ti_3C_2-MXene nanosheets served as the substrate for the binding of hollow gold nanoparticles (HGNPs). HGNPs on the surface of Ti_3C_2-MXene/HGNPs composites were further decorated with staphylococcal protein A (SPA) so that they could conjugate with polyclonal anti-CEA antibodies (Ab_2) termed N-Ti_3C_2-MXene/HGNPs/SPA/Ab_2. N-Ti_3C_2-MXene/HGNPs/SPA/Ab_2 nanoconjugates were then introduced into this SPR sensing system, where they functioned as signal enhancers to further improve the detection sensitivity. The resultant SPR biosensor exhibited a wide linear detection range, ultralow detection limit, and good selectivity toward CEA in human serum. Therefore, the proposed sensing method holds potential in the monitoring of CEA levels for clinical cancer diagnosis and monitoring.

EXPERIMENTAL SECTION

Materials and Reagents. Carcinoembryonic antigen (CEA) and monoclonal and polyclonal anti-CEA were from Fitzgerald Industries. Bovine serum albumin (BSA) was from DingGuo Biotechnology Company. *N*-Hydroxysuccinimide (NHS) and 1-ethyl-3-(3-(dimethylamino)propyl) carbodiimide (EDC) were from JK Chemicals. Hydrogen tetrachloroauratehydrate ($HAuCl_4{\cdot}3H_2O$) was from Acros. The Ti_3AlC_2 MAX phase was from Carbon-Ukraine Ltd. Sodium borohydride ($NaBH_4$), cobalt chloride hexahydrate ($CoCl_2{\cdot}6H_2O$), (3-aminopropyl)triethoxysilane (APTES), hydrofluoric acid, and sodium citrate were from Sinopharm Chemical Reagent Co., Ltd. Human serum samples were from China-Japan Union Hospital of Jilin University. All water used in this experiment was prepared using a Millipore purification device. Anti-CEA and CEA were stored at −20 °C, and other biological reagents were kept at 4 °C. PBS (0.01 mol L^{-1}, pH 7.4, 0.2 g of KCl, 8.0 g of NaCl, 0.24 g of KH_2PO_4, and 1.44 g of Na_2HPO_4 were dissolved in 1000 mL of deionized water) was prepared before use.

Synthesis of Amino-Functionalized Ti_3C_2-MXene Nanosheets. Ti_3C_2-MXene was prepared by etching bulk Ti_3AlC_2 according to a previous method with minor modifications.[34] APTES was used to modify the as-synthesized ultrathin Ti_3C_2-MXene nanosheets with an amino terminal.[35] Typically, 30 mg of Ti_3C_2-MXene was dispersed in 15 mL of ethanol and deionized water (DI water) with a volume ratio of 1:4, after which 200 μL of APTES was slowly dropped into the above solution and stirred at 800 rpm at room temperature for 24 h. The obtained product was washed with DI water several times to remove the unbound APTES, and the purified product underwent vacuum drying overnight at 50 °C. The obtained powder was redispersed in DI water to form a 2 mg mL^{-1} N-Ti_3C_2-MXene solution, which was stored at 4 °C for further use.

Synthesis of Ti_3C_2-MXene/HGNPs/SPA/Ab_2 Nanocomposite. The prepared N-Ti_3C_2-MXene nanosheets were further decorated with HGNPs, which served as SPR signal enhancers. According to Schwartzberg's method, HGNPs were obtained by employing cobalt nanoparticles as the sacrificial templates.[36] The obtained product was harvested by centrifugation and dispersed in 10 mL of DI water. To prepare N-Ti_3C_2-MXene/HGNPs nanohybrids, 6 mL of the as-prepared HGNPs solution was mixed with 10 mL of a 0.4 mg mL^{-1} N-Ti_3C_2-MXene solution, followed by ultrasonication for 30 min under a nitrogen (N_2) atmosphere. The resultant N-Ti_3C_2-MXene/HGNPs nanohybrids were washed three times with DI water, and the final precipitates were redispersed in 12 mL of PBS and stored at 4 °C for further use. To achieve N-Ti_3C_2-MXene/HGNPs/SPA nanocomposites, 200 μL of SPA (1 mg mL^{-1}) was added to 3 mL of the N-Ti_3C_2-MXene/HGNPs nanohybrid solution, which was maintained at 4 °C for 3 h. Afterward, the unbound SPA in the solution was removed by centrifugation, and the obtained N-Ti_3C_2-MXene/HGNPs/SPA nanocomposites were redispersed in 4 mL of PBS. N-Ti_3C_2-MXene/HGNPs/SPA/Ab_2 nanoconjugates were prepared by adding 200 μg of Ab_2 to the above solution, with gentle stirring at room temperature for 12 h. The resultant solution was centrifuged and redispersed in 4 mL of PBS comprising 10 mg mL^{-1} BSA for blocking the nonbinding sites. HGNPs/SPA/Ab_2 nanoconjugates, which served as the control, were prepared by the same procedure used to prepare N-Ti_3C_2-MXene/HGNPs/SPA/Ab_2 nanoconjugates.

Fabrication of Biosensing Platform. The SPR assay in this study was carried out by an angle modulation SPR biosensor based on the conventional Kretchmann configuration. The general instrument details and working principle are provided in the Supporting Information (Figure S1). Shifts of the resonance angle that originated from refractive index changes of the sensing chip surface were measured. A bare gold film was coated on a glass slide and then attached to the bottom of a reactor to serve as the SPR sensing interface. First, 500 μL of a 0.8 mg mL^{-1} N-Ti_3C_2-MXene solution was injected into the flow cell, which was then incubated for 12 h at room temperature to allow the assembly of N-Ti_3C_2-MXene nanosheets on the bare gold film. Subsequently, free N-Ti_3C_2-MXene nanosheets in the solution on the chip surface were washed away with DI water. Afterward, a PBS baseline solution was injected into the flow cell. Here, 500 μL of 100 μg mL^{-1} Ab_1 was activated by EDC (0.2 mol L^{-1}) and NHS (0.05 mol

https://dx.doi.org/10.1021/acs.analchem.9b05372
Anal. Chem. XXXX, XXX, XXX−XXX

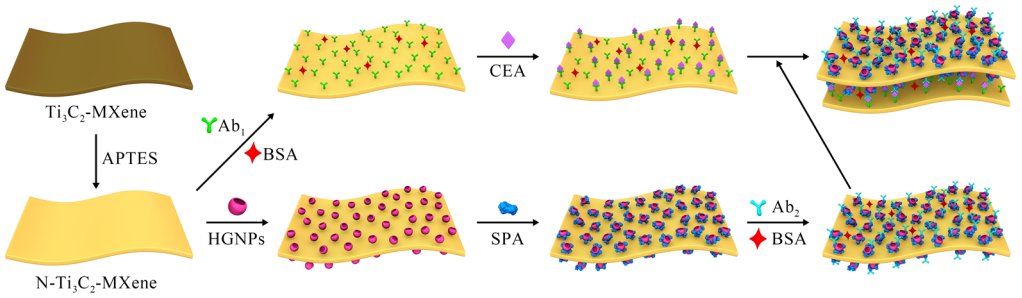

Figure 1. Schematic of detection procedure of the prepared SPR biosensor.

L^{-1}) for 15 min at 4 °C in advance and then was injected into the flow cell. Ab_1 was immobilized on N-Ti_3C_2-MXene nanosheets through the covalent bonding between amino groups of N-Ti_3C_2-MXene nanosheets and carboxyl groups on the Fc region of anti-CEA. The prepared Ab_1/N-Ti_3C_2-MXene/gold film sensing chip was washed by PBS to remove any unbound Ab_1. Then, 10 mg mL^{-1} BSA was injected into the flow cell, which was then incubated for 20 min at room temperature so that BSA could block unspecific active sites on the sensing chip. Finally, PBS was injected to remove the unbound BSA in the flow cell, and the prepared sensing platform was ready for capturing CEA in the samples.

Detection of CEA. For SPR measurement, 500 μL of the CEA sample diluted with PBS was allowed to flow over the surface of the sensing platform and then incubated at room temperature for 30 min. Free CEA in the solution was removed by flowing PBS gently over the sensing chip. After a stable resonant angle was obtained (about 5 min), 500 μL of the N-Ti_3C_2-MXene/HGNPs/SPA/Ab_2 signal enhancer solution was injected into the flow cell and then incubated for 20 min. Finally, unreacted N-Ti_3C_2-MXene/HGNPs/SPA/Ab_2 signal enhancers were washed away with PBS. The biosensor responses were determined as resonance angle shifts before the CEA sample injection and after washing off free signal enhancers. Figure 1 illustrates a schematic representation of the detection process. The entire assay was conducted at room temperature and atmosphere pressure. All measurements were repeated three times to ensure their repeatability.

RESULTS AND DISCUSSION

Characterization. The obtained Ti_3C_2-MXene nanosheets were first analyzed by X-ray diffraction (XRD) to identify their crystal structure (Figure 2a). Several sharp diffraction peaks are located at 6.06°, 18.08°, 30.44°, 36.68°, 43.04°, and 69.4° in the XRD pattern, which is consistent with a previous report.[32] Furthermore, the chemical status of the Ti_3C_2-MXene nanosheets was characterized by typical X-ray photoelectron spectroscopy (XPS). The survey spectrum of Ti_3C_2-MXene illustrates the presence of Ti, C, O, and F, and the O and F correspond to the −OH and F terminal groups on the surface of the Ti_3C_2-MXene nanosheets formed during etching, respectively.[37] APTES functionalization was utilized to prepare N-Ti_3C_2-MXene nanosheets, and the appearances of Si 2p and N 1s peaks confirmed that the Ti_3C_2-MXene nanosheets had been successfully modified (Figure 2b, c). The obvious Au signal in XPS demonstrates the formation of N-Ti_3C_2-MXene/HGNPs nanohybrids. The Au 4f spectrum (Figure 2d) resolved into two spin−orbit components, and these two peaks showed binding energies of 83.5 and 87.2 eV,

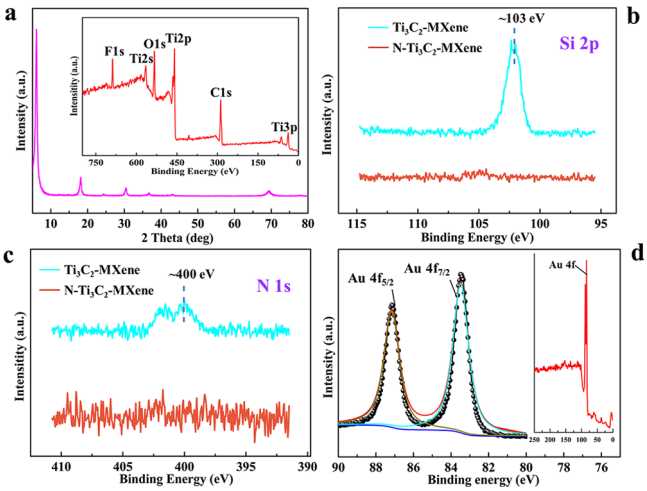

Figure 2. (a) XRD pattern of Ti_3C_2-MXene; (inset) XPS spectrum of Ti_3C_2-MXene. (b), (c) XPS spectra exhibiting the chemical states of Si and N on the surfaces of Ti_3C_2-MXene and N-Ti_3C_2-MXene. (d) High-resolution XPS spectrum of Au 4f.

corresponding to the Au $4f_{7/2}$ and $4f_{5/2}$ peaks of metallic gold, respectively.[38,39]

Structural and Morphological Analysis. Few-layer or single-layer Ti_3C_2-MXene nanosheets were originated from parent MAX-phase ceramics. Very thin, highly transparent, and smooth Ti_3C_2-MXene nanosheets that underwent procedures of delamination, disintegration, and probe sonication breakage are clearly observed in Figure 3a. After APTES functionalization, few N-Ti_3C_2-MXene sheets tended to overlap onto each other, and the smoothness of the sheets degraded due to the shearing forces applied from the stirring process. However, the N-Ti_3C_2-MXene nanosheets were still gauzy based on the TEM image (Figure 3b). According to AFM analysis, the thickness of the prepared N-Ti_3C_2-MXene sheets was 1.9 nm, further confirming the formation of single-layered and few-layered N-Ti_3C_2-MXene nanosheets (Figure 3d). We synthesized HGNPs to prepare N-Ti_3C_2-MXene/HGNPs nanohybrids. The prepared HGNPs, exhibited in Figure S2a and the inset in Figure 3c, were of good structure with an average shell diameter of 43 ± 6 nm and wall thickness of 3 ± 0.4 nm. For the N-Ti_3C_2-MXene/HGNPs nanohybrids, HGNPs exhibited uniform distribution over the ultrathin N-Ti_3C_2-MXene nanosheets (Figure 3c).

Ultraviolet and Visible (UV−vis) Spectroscopy Analysis. Figure S3 shows the UV−vis spectroscopy results for HGNPs, NTi_3C_2-MXene, N-Ti_3C_2-MXene/HGNPs, N-Ti_3C_2-MXene/HGNPs/SPA, and N-Ti_3C_2-MXene/HGNPs/SPA/Ab_2 suspensions. The absorption spectrum of delaminated

https://dx.doi.org/10.1021/acs.analchem.9b05372
Anal. Chem. XXXX, XXX, XXX−XXX

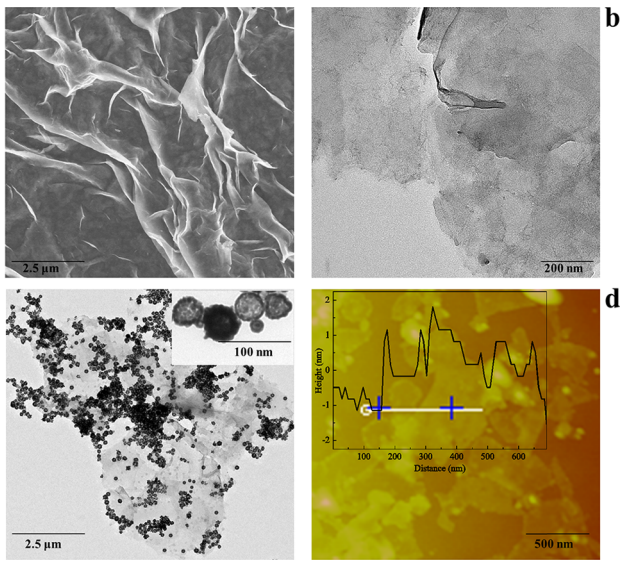

Figure 3. (a) SEM image of as-synthesized 2D Ti_3C_2-MXene nanosheets. (b) TEM image of N-Ti_3C_2-MXene. (c) N-Ti_3C_2-MXene/HGNPs nanohybrids. (d) AFM image of N-Ti_3C_2-MXene.

N-Ti_3C_2-MXene in a dilute aqueous medium exhibited no obvious peaks, and the absorbance of N-Ti_3C_2-MXene decreased monotonically with an increase in the wavelength of incident light in the range of 300−900 nm. The SPR band of N-Ti_3C_2-MXene/HGNPs suspensions appeared in the visible region at 615 nm, which corresponded to the adsorption peak of HGNPs. SPA, a polypeptide of staphylococcus, can form an appropriate linkage between HGNPs and Ab_2 because gold−SPA complexes have a high association constant, and SPA can selectively bind with the Fc regions of antibodies.[40] The absorption peaks of HGNPs in the N-Ti_3C_2-MXene/HGNPs nanohybrids showed obvious red-shifts after the attachment of SPA (630 nm) and Ab_2 (650 nm). These red-shifts demonstrated the change in the localized refractive index near HGNPs, suggesting the successful preparation of N-Ti_3C_2-MXene/HGNPs/SPA/Ab_2 nanoconjugates. For comparison, we prepared HGNPs/SPA/Ab_2 nanoconjugates, and the apparent red-shifts of the bare HGNPs adsorption peak position indicate that HGNPs/SPA/Ab_2 nanoconjugates were successfully fabricated (Figure S2b).

Amino-Functionalized Ti_3C_2-MXene-Based Biosensing Platform. The as-prepared N-Ti_3C_2-MXene nanosheets were demonstrated to be ultrathin and rough with the surface engineering of amino groups, offering large surface areas and high loading capacities of anti-CEA. By virtue of the strong metal−carbon coupling between MXene and the gold chip surface, and adsorption of the amino terminal of N-Ti_3C_2-MXene on the gold surface, 2D N-Ti_3C_2-MXene nanosheets are expected to complete self-assembly on a flat gold film.[41] Different concentrations of N-Ti_3C_2-MXene were injected into the flow cell to assemble on the bare gold film, and DI water was then injected to wash away nonadsorbed N-Ti_3C_2-MXene. The assembly of N-Ti_3C_2-MXene nanosheets on the gold chip was monitored by an SPR technique and could reach saturation within 12 h. An increasing amount of N-Ti_3C_2-MXene nanosheets assembled on the gold film with an increase in N-Ti_3C_2-MXene concentration, leading to the red-shift of a resonance angle. Figure S4 shows the revolution of the SPR curve with regard to the resonance angle and reflectivity when N-Ti_3C_2-MXene sheets were assembled on a bare gold film. The SPR angle shift demonstrated the adsorption of N-Ti_3C_2-MXene onto the gold chip surface. Meanwhile, the decrease in the reflection loss reveals that Ti_3C_2-MXene is an absorbing dielectric medium. The resonance angle shift achieved a maximum value of 0.60° when the concentration of the N-Ti_3C_2-MXene solution increased to 0.8 mg mL^{-1}, suggesting that assembly of N-Ti_3C_2-MXene nanosheets on the gold film had reached saturation (Figure S5a). The corresponding morphological changes of the sensor chip surface were characterized by SEM. As shown in Figure S6, for the concentration of 0.8 mg mL^{-1}, a satisfactory uniform distribution of N-Ti_3C_2-MXene sheets on the gold film was observed, which confirms the successful assembly of the N-Ti_3C_2-MXene sheets on the gold chip. Figure S5b exhibits the SPR spectra of a N-Ti_3C_2-MXene-modified sensing chip before and after 10 washing cycles. The blue-shift of the resonance angle after 10 washing cycles is less than 8% of the initial shift of the resonance angle, demonstrating the stability of N-Ti_3C_2-MXene sheets assembled on the gold film. After modification of the sensing chip, 100 μg mL^{-1} Ab_1 activated by EDC and NHS in advance was introduced into the reactor and immobilized on the N-Ti_3C_2-MXene nanosheets by covalent attachment. The immobilization of Ab_1 on the N-Ti_3C_2-MXene sheets could be completed within 60 min and resulted in a red-shift of about 0.5°.

Analytical Performance of the Biosensor. In this sensing strategy, N-Ti_3C_2-MXene/HGNPs/SPA/Ab_2 nanocomposites were introduced into the sensing system as signal enhancers after CEA was captured on the sensing chip surface to further improve the detection sensitivity of the system. This signal amplification is due to the following reasons: (1) The introduction of N-Ti_3C_2-MXene/HGNPs/SPA/Ab_2 nanoconjugates increases the mass captured on the SPR chip interface and then increases the real part of the refractive index of the chip surface. (2) The strong electromagnetic coupling between the dense HGNPs and the underlying gold chip increases the imaginary part of the refractive index of the sensing chip. Therefore, the amount of N-Ti_3C_2-MXene/HGNPs/SPA/Ab_2 nanoconjugates used in this assay was optimized prior to the detection. A total of 500 μL of an as-prepared N-Ti_3C_2-MXene/HGNPs/SPA/Ab_2 solution diluted with different volumes of PBS was introduced into the proposed sensing system for the detection of 10^{-9} M CEA. The resonance angle displayed an increasing red-shift with the injection of an increasing volume of the N-Ti_3C_2-MXene/HGNPs/SPA/Ab_2 solution up to a final volume of 400 μL, indicating that N-Ti_3C_2-MXene/HGNPs/SPA/Ab_2 nanoconjugates captured on the sensing chip had reached saturation (Figure S7a). Based on this result, the optimum volume of the N-Ti_3C_2-MXene/HGNPs/SPA/Ab_2 solution used in all experiments reported below was 400 μL. With this optimization, the maximum red-shift of the resonance angle obtained a 131% increase over that of the sensing strategy without N-Ti_3C_2-MXene/HGNPs/SPA/Ab_2 signal enhancers.

For quantification of CEA, samples with different concentrations of CEA were determined by the proposed strategy, and the resulting shifts of the resonance angle were measured. Figure 4a and b shows the SPR responses of the proposed biosensing system to CEA samples with different concentrations, and the shifts of the resonance angle gradually increased with the increase in CEA concentrations. The fitting result in Figure 4c reveals that the resonance angle shift ($\Delta\theta$)

https://dx.doi.org/10.1021/acs.analchem.9b05372
Anal. Chem. XXXX, XXX, XXX−XXX

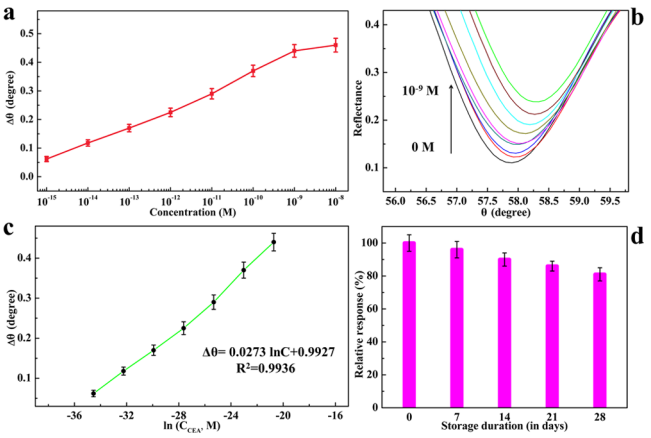

Figure 4. (a) Relationship between SPR angle shifts and concentrations of CEA obtained with the biosensor based on the N-Ti_3C_2-MXene/Ab_1 sensing platform and N-Ti_3C_2-MXene/HGNPs/SPA/Ab_2 signal enhancer. (b) Corresponding SPR spectra with concentrations of CEA ranging from 10^{-15} to $\times10^{-9}$ M. (c) Calibration plot of the magnitudes of the recorded resonance angle shift and natural logarithm of the CEA concentration (ln *C*) obtained with the proposed biosensor. (d) Stability of the N-Ti_3C_2-MXene/Ab_1-based sensing platform. Error bar = ±SD, and n = 3.

exhibited a linear relationship with the logarithm of the CEA concentration from 10^{-15} to 10^{-9} M, which could be described as $\Delta\theta = 0.9927 + 0.0273 \ln C$ (ln *C* is the natural logarithm of the CEA concentration, $R^2 = 0.9936$). The obtained detection limit (S/N = 3) was 0.15 fM. Our biosensor shows advantages both in detection limit and detection range compared with those reported in the literatures (Table 1). Moreover, the fact that the relative standard deviations (RSD) obtained by carrying out independent testing of each sample in triplicate were less than 5% suggests that the proposed method has good reproducibility and stability.

To explore the role of each component in the proposed sensing strategy for improving sensitivity, control experiments of a traditional mercaptopropionic acid (MPA)/Ab_1-modified sensing platform without a signal enhancer, N-Ti_3C_2-MXene/Ab_1-modified sensing platform without a signal enhancer, N-Ti_3C_2-MXene/Ab_1-modified sensing platform with Ab_2 signal enhancers, and N-Ti_3C_2-MXene/Ab_1-modified sensing platform with HGNPs/SPA/Ab_2 nanoconjugates signal enhancers were conducted to determine a 10^{-10} M CEA solution. Similarly, the amount of HGNPs/SPA/Ab_2 was also optimized prior to the assay (Figure S7b). The SPR response signals were effectively amplified owing to the modifications made to the sensing structure (Figure S8). For the sensing chip materials, N-Ti_3C_2-MXene nanosheets with large surface areas provide better capacity of immobilizing Ab_1 compared with traditional MPA modification, which greatly increases the sensitivity of the platform. For further improving the detection sensitivity, the sandwich method was introduced in this assay. Furthermore, performances of Ab_2, HGNPs/SPA/Ab_2, and N-Ti_3C_2-MXene/HGNPs/SPA/Ab_2 signal enhancers were estimated. Introduction of gold nanoparticles which have excellent optical properties, favorable biocompatibility, and outstanding surface modifications to SPR biosensing systems is recognized as an effective way of improving the detection sensitivity of the system. HGNPs showed higher refractive index sensitivity compared with those of solid gold nanostructures owing to the strong plasmonic coupling between the inner and outer surfaces.[42] The electromagnetic coupling between HGNPs and the gold chip greatly amplifies SPR signals. For N-Ti_3C_2-MXene/HGNPs/SPA/Ab_2, HGNPs achieved satisfactory dispersion on the surfaces of N-Ti_3C_2-MXene nanosheets, which eliminated the aggregation of HGNPs due to their high surface energy. Also, N-Ti_3C_2-MXene/HGNPs/SPA/Ab_2 on the sensing film directly increases the mass captured on the sensing chip, resulting in significant sensitivity enhancement. The proposed sensing strategy results in an approximate 6-fold increase in the maximum resonance angle shift over that of the traditional MPA-based sensing strategy.

Stability and Reusability of Sensing Platform. Stability of N-Ti_3C_2-MXene nanosheets is crucial for maintaining its sensing properties. A shelf lifetime investigation of the BSA/Ab_1/N-Ti_3C_2-MXene-modified sensing platform was carried out for detecting CEA (10^{-10} M) at regular intervals of time, during which the prepared sensing chip was kept at 4 °C. A N-Ti_3C_2-MXene-modified sensing chip after storage for 28 days loses 20% of its activity (Figure 4d), indicating that the proposed sensing platform possesses good stability, and amino functionalization of Ti_3C_2-MXene can protect Ti_3C_2-MXene from being oxidized to some extent. In addition, we also examined the reusability of the fabricated biosensor. The prepared sensing chip can be reused after washing its sensing interface with massive PBS containing a large amount of ions. The obtained result reveals that the proposed biosensor still possessed about 84% of its initial activity after five reuse cycles (Figure S9).

Serum Sample Studies. Good selectivity is crucial for the fabricated biosensors in consideration of the need of analyzing real samples. Blank samples without CEA were detected by the proposed biosensor as control experiments to estimate the nonspecific adsorption of N-Ti_3C_2-MXene/HGNPs/SPA/

Table 1. Comparison of Present Work with Others Reported in Literatures for CEA Detection

Method	Detection range (pM)	Detection limit (fM)	ref
Chemiluminescent	6−2950	256	43
FRET	2.5−350	750	44
Electrochemical	0.15−30	700	45
Photoelectrochemical	0.0005−50	0.2995	46
SPR	5−1250	1500	47
SPR	2−125	500	48
SPR	0.5−5000	500	49
SPR	15−2000	15000	50
SPR	5−300	5000	51
SPR	0. 001−1000	0.15	this work

https://dx.doi.org/10.1021/acs.analchem.9b05372
Anal. Chem. XXXX, XXX, XXX−XXX

Table 2. Determination of CEA Concentration in Serum Samples Using the Proposed Biosensor (n = 3)

Content of CEA (pM)	Spiked (pM)	Detected (pM)	Recovery (%)	RSD (%)
none	10	9.58	95.8	7.1
none	1	0.986	98.6	3.4
none	0.01	0.00915	91.5	5.2
none	0.001	0.00104	104	3.9

Ab_2/BSA nanoconjugates on the sensing chip surface. The fact that the resultant resonance angle shift is nearly zero confirms the negligible nonspecific interaction between N-Ti_3C_2-MXene/HGNPs/SPA/Ab_2 signal enhancers and the sensing chip. To evaluate the sensing properties of the N-Ti_3C_2-MXene-based biosensor in real serum samples, SPR responses of CEA spiked-blank serum samples diluted 10 times with PBS were determined by the proposed biosensor. The obtained results exhibited acceptable recoveries ranging from 91.5% to 104% with RSDs of 3.4%−7.1% (Table 2).

Furthermore, the proposed biosensor was tested with actual clinical samples for demonstrating the clinical application of this sensor. Four cancer patients' serum samples including one case of rectal cancer, one case of gastric cancer, and two cases of colon cancer offered by China-Japan Union Hospital of Jilin University were measured by our method. A commercial ELISA kit was also employed as the control. The resultant relative deviations between this sensor and ELISA kit were from 6.15% to 9.21% (Table S1), suggesting that our method holds great promise in the clinical diagnosis of cancer.

CONCLUSIONS

We have fabricated a highly sensitive and selective SPR biosensor for detecting CEA, based on an ultrathin N-Ti_3C_2-MXene/Ab_1 sensing platform and N-Ti_3C_2-MXene/HGNPs/SPA/Ab_2 signal enhancer. Ultrathin Ti_3C_2-MXene nanosheets were prepared and further modified with APTES for the covalent immobilization of Ab_1. N-Ti_3C_2-MXene/HGNPs/SPA conjugated with Ab_2 was utilized as response signal enhancers to further improve the detection sensitivity. The fabricated biosensor exhibited a wide detection range of 0.001−1000 PM with a detection limit of 0.15 fM. The CEA concentration in serum samples has been estimated by using the proposed sensing strategy to evaluate the clinical application of this sensor. The high recoveries of spiked blank serum samples highlight the good selectivity of the proposed method for biomolecules in complex mixtures. Greater effort should be expended to prevent oxidation of N-Ti_3C_2-MXene for further extending the quality guarantee period of the N-Ti_3C_2-MXene-based sensing chip. Our work on introducing Ti_3C_2-MXene-based SPR sensing chip material for CEA detection broadens the application fields of MXenes. We believe that the proposed ultrathin Ti_3C_2-MXene holds great potential in biosensing and biomedical fields.

ASSOCIATED CONTENT

Supporting Information

The Supporting Information is available free of charge at https://pubs.acs.org/doi/10.1021/acs.analchem.9b05372.

Photograph of the angle modulation SPR analyzer; SEM image and SPR spectrum of N-Ti_3C_2-MXene nanosheets assembled on gold film; stability measurement; UV−vis spectra characterization and amount optimization of HGNPs/SPA/Ab_2 and N-Ti_3C_2-MXene/HGNPs/SPA/Ab_2 nanoconjugates; detection performance based on different sensing strategies; repeatability of the prepared sensor chip; and real sample analysis. (PDF)

AUTHOR INFORMATION

Corresponding Authors

Xuedong Fang − *Department of Gastrointestinal and Colorectal Surgery, China-Japan Union Hospital of Jilin University, Changchun 130033, Jilin, China*; Phone: +86-431-85155279; Email: fangxd1961@163.com; Fax: +86-431-85155279

Fangfang Chen − *Department of Gastrointestinal and Colorectal Surgery, China-Japan Union Hospital of Jilin University, Changchun 130033, Jilin, China*; Phone: +86-431-85155279; Email: cff@jlu.edu.cn; Fax: +86-431-85155279

Xiaoqiang Cui − *State Key Laboratory of Automotive Simulation, School of Materials Science and Engineering, and Control and Key Laboratory of Automobile Materials of MOE, Jilin University, Changchun 130012, Jilin, China*; orcid.org/0000-0002-5858-6257; Phone: +86-431-85155279; Email: xqcui@jlu.edu.cn; Fax: +86-431-85155279

Authors

Qiong Wu − *State Key Laboratory of Automotive Simulation, School of Materials Science and Engineering, and Control and Key Laboratory of Automobile Materials of MOE, Jilin University, Changchun 130012, Jilin, China; Department of Gastrointestinal and Colorectal Surgery, China-Japan Union Hospital of Jilin University, Changchun 130033, Jilin, China*

Ningbo Li − *State Key Laboratory of Automotive Simulation, School of Materials Science and Engineering, and Control and Key Laboratory of Automobile Materials of MOE, Jilin University, Changchun 130012, Jilin, China*

Ying Wang − *State Key Laboratory of Automotive Simulation, School of Materials Science and Engineering, and Control and Key Laboratory of Automobile Materials of MOE, Jilin University, Changchun 130012, Jilin, China*

Yanchao Xu − *State Key Laboratory of Automotive Simulation, School of Materials Science and Engineering, and Control and Key Laboratory of Automobile Materials of MOE, Jilin University, Changchun 130012, Jilin, China*

Jiandong Wu − *State Key Laboratory of Automotive Simulation, School of Materials Science and Engineering, and Control and Key Laboratory of Automobile Materials of MOE, Jilin University, Changchun 130012, Jilin, China*

Guangri Jia − *State Key Laboratory of Automotive Simulation, School of Materials Science and Engineering, and Control and Key Laboratory of Automobile Materials of MOE, Jilin University, Changchun 130012, Jilin, China*

Fujian Ji − *Department of Gastrointestinal and Colorectal Surgery, China-Japan Union Hospital of Jilin University, Changchun 130033, Jilin, China*

Complete contact information is available at: https://pubs.acs.org/10.1021/acs.analchem.9b05372

Notes

The authors declare no competing financial interest.

https://dx.doi.org/10.1021/acs.analchem.9b05372
Anal. Chem. XXXX, XXX, XXX−XXX

■ ACKNOWLEDGMENTS

We greatly acknowledge the National Postdoctoral Program for Innovative Talents (BX20180117), Jilin Province Science and Technology Development Program (20190201233JC), National Key Research and Development Program of China (2016YFA0200400), National Natural Science Foundation of China (51571100, 51872116, 51702116, 51602305, and 31771093), Program for JLU Science and Technology Innovative Research Team (JLUSTIRT, 2017TD-09, 2017TD-27, 2019TD-36), and Project of International Collaboration of Jilin Province (201180414085GH).

■ REFERENCES

(1) Li, N. L.; Jia, L. P.; Ma, R. N.; Jia, W. L.; Lu, Y. Y.; Shi, S. S.; Wang, H. S. *Biosens. Bioelectron.* **2017**, *89*, 453−460.
(2) Yoon, J. H.; Ham, I. H.; Kim, O.; Ashktorab, H.; Smoot, D. T.; Nam, S. W.; Lee, J. Y.; Hur, H.; Park, W. S. *Gastric Cancer* **2018**, *21*, 956−967.
(3) Zhang, X.; Peng, J.; Song, Y.; Chen, Y.; Lu, F.; Gao, W. *Biosens. Bioelectron.* **2019**, *133*, 125−132.
(4) Wang, Y.; Wei, Z.; Luo, X.; Wan, Q.; Qiu, R.; Wang, S. *Talanta* **2019**, *195*, 33−39.
(5) Jie, G.; Ge, J.; Gao, X.; Li, C. *Biosens. Bioelectron.* **2018**, *118*, 115−121.
(6) Shang, B. B.; Li, X.; Zhang, X. R.; Huang, W. S.; Qi, B. P.; Zhou, C. H. *Bioelectrochemistry* **2019**, *129*, 278−285.
(7) Zhao, J.; Liang, D.; Gao, S.; Hu, X.; Koh, K.; Chen, H. *Biosens. Bioelectron.* **2019**, *141*, 111440.
(8) Peng, D.; Kavanagh, O.; Gao, H.; Zhang, X.; Deng, S.; Chen, D.; Liu, Z.; Xie, C.; Situ, C.; Yuan, Z. *Food Chem.* **2020**, *302*, 124623.
(9) Li, Q.; Dou, X.; Zhang, L.; Zhao, X.; Luo, J.; Yang, M. *Anal. Bioanal. Chem.* **2019**, *411*, 6057−6066.
(10) Souto, D. E. P.; Volpe, J.; Goncalves, C. C.; Ramos, C. H. I.; Kubota, L. T. *Talanta* **2019**, *205*, 120122.
(11) Zeng, S.; Baillargeat, D.; Ho, H. P.; Yong, K. T. *Chem. Soc. Rev.* **2014**, *43*, 3426−3452.
(12) Su, S.; Sun, Q.; Gu, X.; Xu, Y.; Shen, J.; Zhu, D.; Chao, J.; Fan, C.; Wang, L. *TrAC, Trends Anal. Chem.* **2019**, *119*, 115610.
(13) Patil, P. O.; Pandey, G. R.; Patil, A. G.; Borse, V. B.; Deshmukh, P. K.; Patil, D. R.; Tade, R. S.; Nangare, S. N.; Khan, Z. G.; Patil, A. M.; More, M. P.; Veerapandian, M.; Bari, S. B. *Biosens. Bioelectron.* **2019**, *139*, 111324.
(14) Mahmoudpour, M.; Ezzati Nazhad Dolatabadi, J.; Torbati, M.; Homayouni-Rad, A. *Biosens. Bioelectron.* **2019**, *127*, 72−84.
(15) Fathi, F.; Rashidi, M. R.; Omidi, Y. *Talanta* **2019**, *192*, 118−127.
(16) Mohammadzadeh-Asl, S.; Keshtkar, A.; Ezzati Nazhad Dolatabadi, J.; de la Guardia, M. *Biosens. Bioelectron.* **2018**, *110*, 118−131.
(17) Primo, E. N.; Kogan, M. J.; Verdejo, H. E.; Bollo, S.; Rubianes, M. D.; Rivas, G. A. *ACS Appl. Mater. Interfaces* **2018**, *10*, 23501−23508.
(18) Kaushik, S.; Tiwari, U. K.; Pal, S. S.; Sinha, R. K. *Biosens. Bioelectron.* **2019**, *126*, 501−509.
(19) Srivastava, T.; Jha, R. *IEEE Photonics Technol. Lett.* **2018**, *30*, 319−322.
(20) Xue, T.; Liang, W.; Li, Y.; Sun, Y.; Xiang, Y.; Zhang, Y.; Dai, Z.; Duo, Y.; Wu, L.; Qi, K.; Shivananju, B. N.; Zhang, L.; Cui, X.; Zhang, H.; Bao, Q. *Nat. Commun.* **2019**, *10*, 28.
(21) Shpigel, N.; Levi, M. D.; Sigalov, S.; Mathis, T. S.; Gogotsi, Y.; Aurbach, D. *J. Am. Chem. Soc.* **2018**, *140*, 8910−8917.
(22) Persson, I.; Halim, J.; Lind, H.; Hansen, T. W.; Wagner, J. B.; Naslund, L. A.; Darakchieva, V.; Palisaitis, J.; Rosen, J.; Persson, P. O. A. *Adv. Mater.* **2019**, *31*, 1805472.
(23) Lin, H.; Chen, Y.; Shi, J. *Adv. Sci.* **2018**, *5*, 1800518.
(24) Sinha, A.; Dhanjai; Zhao, H.; Huang, Y.; Lu, X.; Chen, J.; Jain, R. *TrAC, Trends Anal. Chem.* **2018**, *105*, 424−435.
(25) Sun, W.; Wang, X.; Feng, J.; Li, T.; Huan, Y.; Qiao, J.; He, L.; Ma, D. *Nanotechnology* **2019**, *30*, 385601.
(26) Chen, J.; Tong, P.; Huang, L.; Yu, Z.; Tang, D. *Electrochim. Acta* **2019**, *319*, 375−381.
(27) Li, W.; Song, Z.; Zhong, J.; Qian, J.; Tan, Z.; Wu, X.; Chu, H.; Nie, W.; Ran, X. *J. Mater. Chem. C* **2019**, *7*, 10371−10378.
(28) Zhou, H.; Lu, Y.; Wu, F.; Fang, L.; Luo, H.; Zhang, Y.; Zhou, M. J. *J. Alloys Compd.* **2019**, *802*, 259−268.
(29) Liu, H.; Zhang, X.; Zhu, Y.; Cao, B.; Zhu, Q.; Zhang, P.; Xu, B.; Wu, F.; Chen, R. *Nano-Micro Lett.* **2019**, *11*, 65.
(30) Wang, H.; Li, H.; Huang, Y.; Xiong, M.; Wang, F.; Li, C. *Biosens. Bioelectron.* **2019**, *142*, 111531.
(31) Zhang, H.; Wang, Z.; Zhang, Q.; Wang, F.; Liu, Y. *Biosens. Bioelectron.* **2019**, *124−125*, 184−190.
(32) Wu, L.; Lu, X.; Dhanjai; Wu, Z. S.; Dong, Y.; Wang, X.; Zheng, S.; Chen, J. *Biosens. Bioelectron.* **2018**, *107*, 69−75.
(33) Kurapati, R.; Kostarelos, K.; Prato, M.; Bianco, A. *Adv. Mater.* **2016**, *28*, 6052−6074.
(34) Alhabeb, M.; Maleski, K.; Anasori, B.; Lelyukh, P.; Clark, L.; Sin, S.; Gogotsi, Y. *Chem. Mater.* **2017**, *29*, 7633−7644.
(35) Kumar, S.; Lei, Y.; Alshareef, N. H.; Quevedo-Lopez, M. A.; Salama, K. N. *Biosens. Bioelectron.* **2018**, *121*, 243−249.
(36) Schwartzberg, A. M.; Olson, T. Y.; Talley, C. E.; Zhang, J. Z. *J. Phys. Chem. B* **2006**, *110*, 19935−19944.
(37) Naguib, M.; Kurtoglu, M.; Presser, V.; Lu, J.; Niu, J.; Heon, M.; Hultman, L.; Gogotsi, Y.; Barsoum, M. W. *Adv. Mater.* **2011**, *23*, 4248−4253.
(38) Hedman, J; Klasson, M; Nilsson, R; Nordling, C; Sorokina, M F; Kljushnikov, O I; Nemnonov, S A; Trapeznikov, V A; Zyryanov, V G *Phys. Scr.* **1971**, *4*, 195−201.
(39) Turner, N. H.; Single, A. M. *Surf. Interface Anal.* **1990**, *15*, 215−222.
(40) Tang, D. P.; Yuan, R.; Chai, Y. Q. *Bioprocess Biosyst. Eng.* **2006**, *28*, 315−321.
(41) Song, B.; Li, D.; Qi, W.; Elstner, M.; Fan, C.; Fang, H. *ChemPhysChem* **2010**, *11*, 585−589.
(42) Mahmoud, M. A.; O'Neil, D.; El-Sayed, M. A. *Chem. Mater.* **2014**, *26*, 44−58.
(43) Chen, Z.; Li, P.; Zhang, Z.; Zhai, X.; Liang, J.; Chen, Q.; Li, K.; Lin, G.; Liu, T.; Wu, Y. *Anal. Chem.* **2019**, *91*, 5777−5785.
(44) Zhang, Y.; Ye, W.; Yang, C.; Xu, Z. *Talanta* **2019**, *205*, 120096.
(45) Tavares, A. P. M.; Truta, L. A. A. N. A.; Moreira, F. T. C.; Carneiro, L. P. T.; Sales, M. G. F. *Biosens. Bioelectron.* **2019**, *140*, 111320.
(46) Huang, D.; Wang, L.; Zhan, Y.; Zou, L.; Ye, B. *Biosens. Bioelectron.* **2019**, *140*, 111358.
(47) Guo, C.; Su, F.; Song, Y.; Hu, B.; Wang, M.; He, L.; Peng, D.; Zhang, Z. *ACS Appl. Mater. Interfaces* **2017**, *9*, 41188−41199.
(48) Springer, T.; Homola, J. *Anal. Bioanal. Chem.* **2012**, *404*, 2869−2875.
(49) Wang, H.; Wang, X.; Wang, J.; Fu, W.; Yao, C. *Sci. Rep.* **2016**, *6*, 33140.
(50) Altintas, Z.; Uludag, Y.; Gurbuz, Y.; Tothill, I. E. *Talanta* **2011**, *86*, 377−383.
(51) Li, R.; Feng, F.; Chen, Z. Z.; Bai, Y. F.; Guo, F. F.; Wu, F. Y.; Zhou, G. *Talanta* **2015**, *140*, 143−149.

https://dx.doi.org/10.1021/acs.analchem.9b05372
Anal. Chem. XXXX, XXX, XXX−XXX